Colegio de
Postgraduados

Photodegradation Diuron herbicide with TiO$_2$-Al$_2$O$_3$ catalysts supported on graphene nanoplatelets

González-Ramón, M.E.1; Cervantes-Uribe, A.1 [iD]; Labrada-Delgado, G. J.2 [iD]; Sierra-Gómez, U.A.3 [iD]; Fernández-Tavizón, S.3; Herrera-Franco, P.J.4 [iD]; Espinosa-González, C.G.5* [iD]

1   División Académica de Ciencias Básicas, Universidad Juárez Autónoma de Tabasco. Km. 1 Carretera Cunduacán-Jalpa de Méndez, La Esmeralda, C. P. 86690, Cunduacán Tabasco, México. adrian.cervantes@ujat.mx
2   Laboratorio Nacional de Investigaciones en Nanociencia y Nanotecnología, Instituto Potosino de Investigación Científica y Tecnológica A.C. Camino a la Presa de San José 2055, Lomas 4ta, C.P. 78216 San Luis Potosí, S.L.P., México. gladis.labrada@ipicyt.edu.mx
3   Laboratorio Nacional de Materiales Grafénicos, Centro de Investigación en Química Aplicada. Enrique Reyna Hermosillo 140, San José de los Cerritos, C.P. 25294, Saltillo Coahuila, México. uriel.sierra@ciqa.edu.mx
4   Unidad de Materiales Avanzados, Centro de Investigación Científica de Yucatán. Calle 43 No. 130 por 32 y 34, Chuburná de Hidalgo, C.P. 97205, Mérida Yucatán, México. pherrera@cicy.mx
5   Investigadoras e Investigadores por México-División Académica de Ciencia Básicas-Universidad Juárez Autónoma de Tabasco. Km. 1 Carretera Cunduacán-Jalpa de Méndez, La Esmeralda, C.P. 86690, Cunduacán Tabasco, México.
*   Correspondence: cgespinosa@conacyt.mx

ABSTRACT
Objective: To photodegrade Diuron with TiO$_2$-Al$_2$O$_3$ nanomaterials supported on graphene nanoplatelets (GnPs)

Design/methodology/approach: The synthesis of the materials was carried out by the sol-gel method under mild conditions. Subsequently, the obtained materials were subjected to thermal processing for structural stabilization and pulverized. Synthesized nanomaterials were then characterized by nitrogen adsorption/desorption, X-ray diffraction, scanning electron microscopy, and Uv-Vis spectroscopy.

Results: The adsorption/desorption results indicated that the ternary TiO$_2$-Al$_2$O$_3$/GnPs nanomaterials were found to have complex porosity, which suggested that TiO$_2$-Al$_2$O$_3$ was formed on agglomerated GnPs. X-ray diffraction data revealed that the anatase phase of TiO$_2$ and the -Al$_2$O$_3$ phase coexist with the crystalline phase of graphene. The morphology of the materials indicates that the nanoplatelets were randomly dispersed in a continuous mixed oxide phase. About the UV analysis, the presence of GnPs at 1 wt % concentration reduces the band gap by 6%.

Limitations on study/implications: The physical and chemical properties of GnPs make the material an excellent candidate for the degradation of pollutants by photocatalysis.

Findings/conclusions: The addition of GnPs improved the Diuron degradation, probably by forming a nanostructured interface or heterojunction.

Keywords: Diuron, GnPs, TiO$_2$, Al$_2$O$_3$, Photocatalysis.

INTRODUCTION

Pesticides and herbicides are continuously used for pest control. Herbicides are classified: 1) according to their interaction with plants, which can be by direct contact and translocation through the soil, 2) by their total or partial effect on vegetation, and 3) their chemical composition. Diuron (1,1-dimethyl, 3-(3', 4'-dichlorophenyl) urea) is a broad-spectrum herbicide and algaecide used in agriculture for weed and algae control especially in and around water bodies (Malato *et al.*, 2003) it inhibits photosynthesis by preventing oxygen production and blocks electron transfer at the plant photosystem level (Wessels, J.S.C. & Van der Veen, R., 1956). This chemical compound has been used to control the growth of a wide variety of seasonal weeds (Giacomazzi & Cochet, 2004). However, compound agriculture has resulted in the contamination of soil and aquatic environments by leaching (Thurman *et al.*, 2000). Furthermore, synthetic herbicides in agriculture in the last ten years have caused significant damage to the ecosystem due to specific physicochemical properties (resistance to biodegradation, toxicity, and solubility, among others) (Fenoll *et al.*, 2013) . For this reason, there is an earnest effort to optimize removal techniques, either by chemical or physical degradation. Among the known techniques, advanced oxidation processes and photodegradation via solar energy are famous (Bamba *et al.*, 2008). On the other hand, semiconductor compounds are used as catalysts for the photodegradation of pollutants. In this area, TiO_2 is widely studied mainly because of its low cost and availability in addition to its physicochemical properties and a favorable redox capacity. Three crystalline forms of TiO_2 have been reported, however, the anatase phase is more active when compared to rutile and brookite (Escobar *et al.*, 2000) (Navarrete *et al.*, 1996) (Araña *et al.*, 2008). Despite its excellent qualities, titanium oxide has a disadvantage, electron-hole recombination. The adverse effects of titanium oxide are inhibited by combining it with other metal oxides and even doping it. Among the examples reported is [Ru(bipy)$_3$] Cl_2-doped with TiO_2/SiO_4, used for wastewater degradation, obtaining 70% efficiency. The materials performed well during photodegradation, and their activity was four times higher than known commercial materials (Bernardes *et al.*, 2016). Graphene oxide (GO) based photocatalyst GO-TiO_2, was investigated under UV-Vis in the photodegradation of a mixture of four pollutants, including Diuron and the results showed a reasonable rate of photodegradation of pesticides in both natural and ultrapure water (M. Cruz *et al.*, 2017). For nanostructured $TiO_2/ZnO/rGO$ (TZR) composites, 5% rGO gave the highest photocatalytic activation (99%) concerning the pure individual components; the rGO load on the TZR composite has attributed an effect on its photocatalytic activation (Nguyen *et al.*, 2020). Boron-doped TiO_2 did not produce a significant degradation of different pesticides studied; even so, a slight decrease in the concentration was observed for the solutions studied (Rey *et al.*, 2015) . Tungsten-doped titanium oxide (W) was tested in the degradation of Diuron under simulated solar irradiation. The best nanophotocatalyst $W_{0.03}Ti_{0.9}7O_2$ showed 70% degradation w.r.t. pure TiO_2 (Publishing & Science, 2017). In another study, TiO_2 doped with 0.5 wt% Sm^{3+} had mesmerizing photocatalytic activity performance for Diuron degradation by sunlight but it was low (42%), and 0.3 wt% Sm^{3+} showed the best performance in photodegradation with Diuron (80%) (D. De Cruz *et al.*, 2011). The work of multiple researchers to discover processes that are more efficient in

photodegradation has led them to combine Al_2O_3 and TiO_2 and achieve a mixed oxide that increases the photocatalytic activity by increasing the contact surface with the molecule to be degraded, so it is considered an excellent binary system for efficient degradation of organic molecules (Anderson & Bard, 1997) (Choi *et al.*, 2006). This research aimed to synthesize and characterize nanostructured ternary materials based on TiO_2, Al_2O_3, and GnPs and correlate the resulting physicochemical properties with the photodegradation efficiency of Diuron.

MATERIALS AND METHODS

Reagents

XG Sciences Inc.'s GnPs, (xGnP®) are nanoparticles consisting piles of a few graphene sheets, single graphene sheets, and nanostructured graphite; the average surface area is 750 $m^2 g^{-1}$. This material is Grade C, typically consisting of platelets with a particle diameter of fewer than 2 m and a few nm thicknesses

Catalyst synthesis

The synthesis method for the materials was sol-gel, which consists of placing graphene nanoplatelets (GnPs) with titanium and/or aluminium precursors in a three-hole flask. With an addition funnel, a 50:50 water-ethanol mixture was added drop by drop, and then, the mixture reaction was heated at 60 °C, maintaining agitation and with constant reflux for 24 h. Later, the reaction product was dried in the rotary evaporator and then placed in an oven at 80 °C for 12 h. Finally, the material was calcined at 500 °C for 4 h with airflow and a heating ramp of 2 °/min^{-1}.

Catalytic Evaluation

A 30 mg kg^{-1} solution was prepared, and 250 mL was poured into the reactor. The catalyst was added to achieve a concentration of 0.4 g L^{-1} and left in agitation for 30 min in the absence of light to reach equilibrium. Subsequently, a first sample was taken before turning on the lamp. It was left in visible irradiation, and 6 mL were taken at 5, 15, 30, 30, 45, 60, 120, 180, 240, and 300 min. From the corresponding calibration curve, UV-Vis readings of the samples were taken. For determining degradation percentages using the following equation: $x(\%) = ([A°] - [A])/[A°]$. Where $(mg\ kg^{-1})$ is the concentration when the light is turned on to start the photodegradation process and $(mg\ kg^{-1})$ is the concentration after five hours under irradiation (Richard Felder, 2004).

Characterization

Nitrogen physisorption: This characterization was carried out in the Micrometrics equipment model Tristar II. First, degassing treatment with nitrogen flow was given to each sample, and then, a liquid nitrogen cooling at -196 °C was supplied.

SEM: This characterization was performed in a Field Emission Scanning Electron Microscope FE SEM FEI Tecnai F30 (300 keV) vacuum of 80 Pa.

X-Ray diffraction: Diffractograms were obtained with a BRUKER diffractometer model D-8, with a Cu Kα radiation $\lambda = 1.54059$ Å, 300 W.

Solid UV-Vis: Readings were carried out in an UV-Vis Cary 300 equipment in a beam range from 200 to 800 nm wavelength at room temperature.

RESULTS AND DISCUSSION

Isotherms represent the volume of nitrogen physisorbed in the solid w.r.t. the relative pressure of nitrogen, because of the adsorption and desorption process of the gas in the solid (Figure 1). The adsorption-desorption isotherms for TiO_2, Al_2O_3, and GnPs materials presented V-type, indicating weak interactions between the adsorbate and adsorbent. The hysteresis loop for GnPs was of H3 type characteristic of plate-like materials. Meanwhile for TiO_2 and Al_2O_3 samples, the hysteresis loop was H5, characteristic of partially blocked mesoporous materials, according to the IUPAC classification (Cychosz *et al.*, 2017).

The pore diameter distribution in samples was calculated from the BJH method. GnPs have a distribution between 400 to 50 nm, with a maximum of 150 nm. TiO_2 and Al_2O_3 samples presented bimodal distribution with maximal diameters centered at 65 and 88 nm, respectively (Figure 1B). Specific surface area was obtained with the BET method; the results are shown in Table 1. The area of GnPs and Al_2O_3 samples are in the typically published ranges (Daş *et al.*, 2019), (Tang *et al.*, 2020). For TiO_2, the surface area depends on the sol-gel synthesis conditions; areas between 50-90 m^2 g^{-1} have been reported in the literature (Tahir *et al.*, 2020).
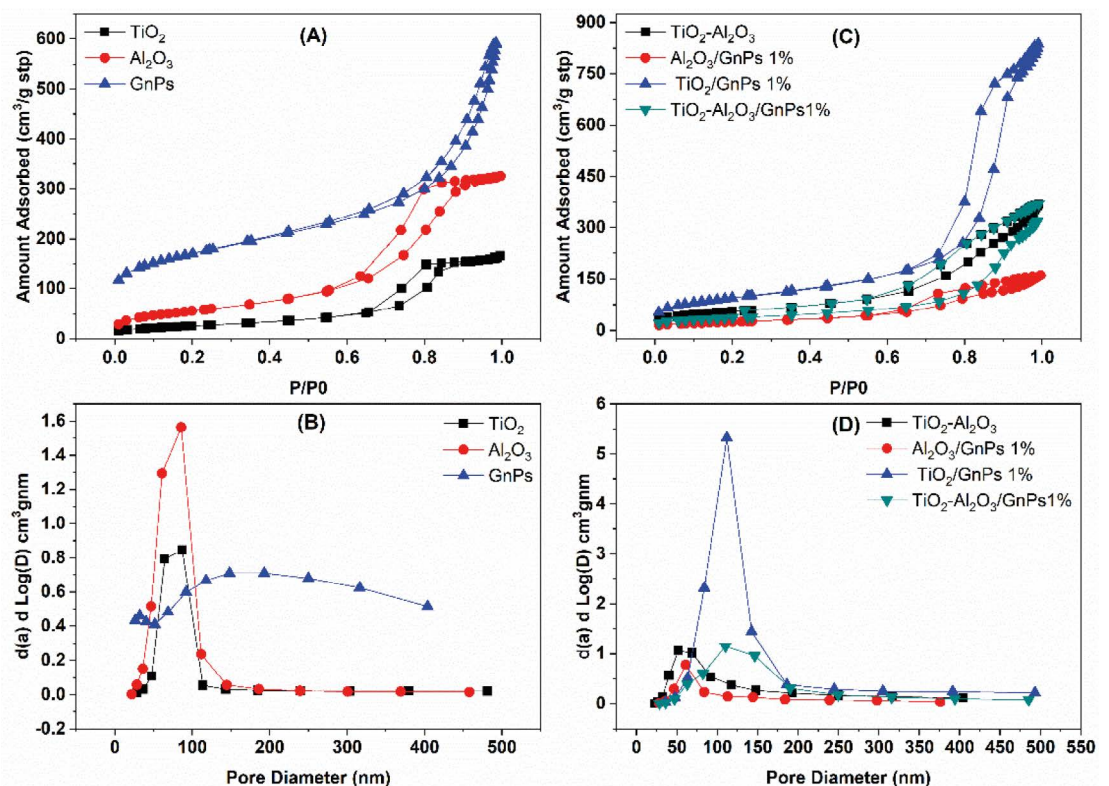

Figure 1. Nitrogen adsorption/dissociation as a function of relative pressure (P/P0) nitrogen for reference materials (A), incorporation of GnPs (C) and pore size distribution of reference (B) and with GnPs (D).

Type (IV) isotherm for TiO_2-Al_2O_3 composite was identified, the pore shape was modified compared to pure composites (TiO_2 and Al_2O_3), and the hysteresis loop was H3. The incorporation of 1% GnPS (TiO_2/GnPs 1%) showed the same isotherm and hysteresis loop as the TiO_2 sample. There was no change in the isotherm type in the case of the Al_2O_3/GnPs 1% sample, but the hysteresis type changed from H3 to H4. This loop is caused by the presence of micro and mesoporosity which is typically observed in carbon-based materials. The combination of the three species resulted in an isotherm type (IV) and a hysteresis loop H2b which represents materials with complex porosity and pore networks connected with bottle-shaped pores (Figure 1C).

Pore diameter distribution was unimodal for Al_2O_3/GnPs 1% and TiO_2/GnPs 1%, with an average diameter of 61 and 112 nm, respectively. TiO_2-Al_2O_3 and TiO_2-Al_2O_3/ GnPs 1% materials presented bimodal distribution with diameters 53-70 and 110-148 nm, respectively (Figure 1D). The addition of GnPs 1% to TiO_2 decreased the surface area by 3.2%; however, this same addition to Al_2O_3 was favored and increased by 68%. The TiO_2-Al_2O_3 composite presented a higher surface area (199 $m^2\,g^{-1}$) than the pure TiO_2. However, the surface area for the TiO_2-Al_2O_3/GnPs 1% composite (131 m2 g-1) is lower to that of TiO2-Al2O3 material since TiO2-Al2O3 was formed and grown on agglomerated GnPs (Table 1).

Results of the X-ray diffraction analysis of the TiO_2, Al_2O_3, and GnPs samples are shown in Figure 2A. GnPs diffraction pattern corroborated that they are grade C graphene nanoplatelets (See annexes). According to the diffraction signal at $2\theta=25.5°$, corresponds to a crystalline graphitic material with few layers. Aluminum oxide showed diffraction signals at $2\theta=37.38$ and $45.98°$, characteristic of the γ-Al_2O_3 phase (Campos *et al.*, 2013). Titanium oxide presented diffractions at $2\theta=25.39$, 38.03, and 48.19°, characteristic of the anatase phase according to JCODS Chart No. 21-1272 (Urbano *et al.*, 2011) .

Results of the binary samples (Al_2O_3/GnPs 1wt%, TiO_2/GnPs 1 wt %) obtained by the sol-gel method are shown in Figure 2B. Characteristic diffraction signals of GnPs and γ-Al_2O_3 were identified for the Al_2O_3/GnPs 1% sample. In case of TiO_2/GnPs 1wt% sample, anatase diffraction signals were superimposed with the signals of GnPs at $2\theta=25°$. A weak signal at $2\theta=30.88°$ corresponding to the brookite structure was also observed.

Table 1. Specific Brunauer-Emmett-Teller (BET) area, volume, and pore size of the reference samples and obtained composite materials.

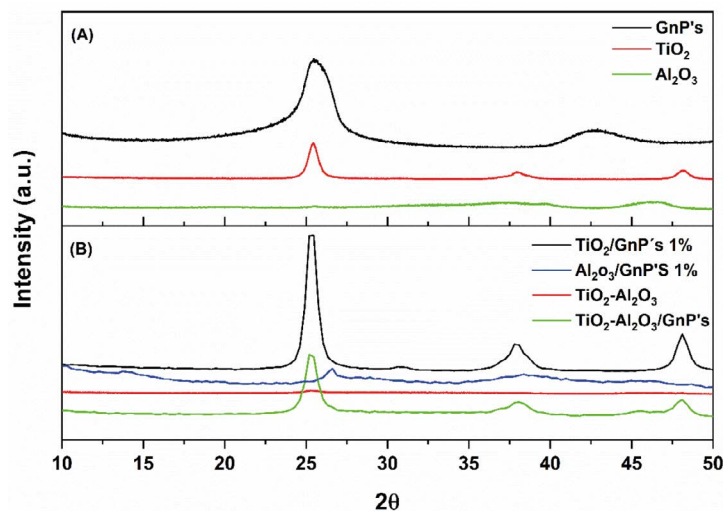| Sample	Surface area $(m^2\,g^{-1})$	Pore volume $(cm^3\,g^{-1})$	Pore size (nm)
TiO_2	93	0.25	7
Al_2O_3	203	0.50	6
GnPs	598	0.72	8
TiO_2-Al_2O_3	199	0.55	8
TiO_2/GnPs 1%	90	0.24	6
Al_2O_3/GnPs 1%	341	1.25	10
TiO_2-Al_2O_3/GnPs 1%	131	0.48	10

Figure 2. Diffractograms for reference samples (A) and samples with 1% GnPs (B).

Figure 2B shows diffractograms of the ternary and binary mixture of the materials. Both mixtures showed characteristic patterns of anatase phase of TiO_2 at $2\theta=25.35$, 38.13, and 48.19°, a slight diffraction signal at $2\theta=45.33°$ corresponding to γ-Al_2O_3. In addition, overlap with the signal corresponding to the 002 planes of GnPs at $2\theta=25.35°$ was also identified. The intensity of the diffraction signals corresponding anatase phase of the ternary mixture was much higher than that of the binary sample because of the more highly ordered phases. Table 1 shows the crystal size of the materials obtained from the Scherrer equation (Scherrer & Hillberry, 1978).

According to the data in Table 2, the addition of GnPs to TiO_2 stabilizes the brookite structural phase and decreases the crystal size. The Al_2O_3/GnPs 1% sample showed no significant change in the gamma-alumina structure, except the increase in the crystal size. Finally, in the TiO_2-Al_2O_3/GnPs 1% sample, despite with the high concentrations of aluminum oxide and simultaneous presence of the graphene crystalline phase, the anatase structure prevails without altering the interplanar distance of the graphitic layers. Therefore, to incorporate GnPs into the TiO_2-Al_2O_3 mixture, serves as stabilizing support.

The field emission scanning electron microscopy technique was used and provided highly focused images, through which morphology and constituents' arrangement of the TiO_2/GnPs, Al_2O_3/GnPs, and TiO_2-Al_2O_3/GnPs materials, were studied.

Figure 3A shows a 4.4 μm cluster, which is constituted by graphitic piles of length between 300 and 44 nm (Figure 3B).

Figure 4A shows TiO_2 dispersed clusters of between 1 and 11 μm, formed from semispherical conglomerates of titanium oxide. Figure 4B shows these conglomerates with semisphere sizes between 1.7 and 1.8 μm.

Micrographs of the Al_2O_3/GnPs 1% sample suggest a morphology characterized by irregular particles of different sizes, see Figure 5A. The observation and arrangement of the GnPs in Figure 5B are difficult to determine; Al_2O_3 probably covers them.
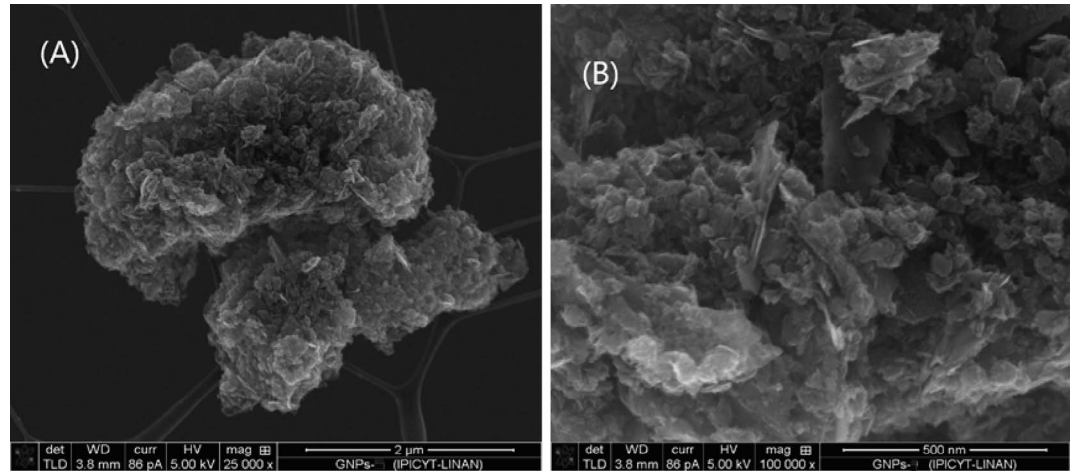
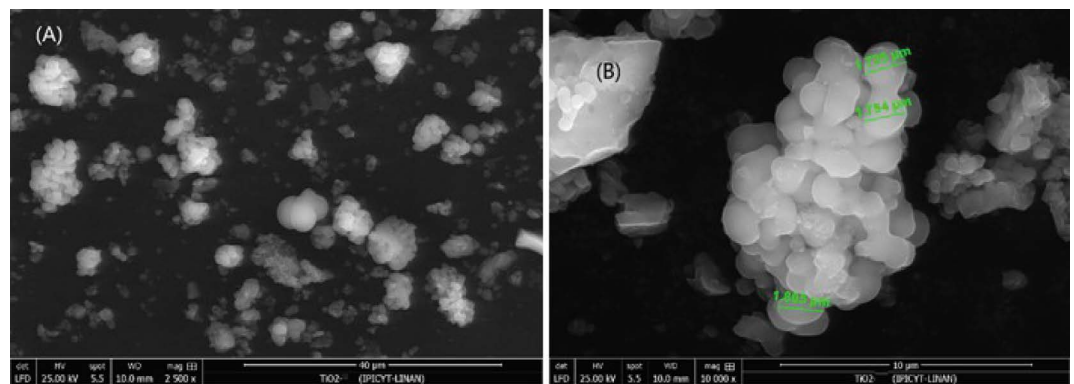**Figure 3**. SEM micrographs of graphene nanoplatelets (GnPs) at 25 000X and 100 000X magnification.

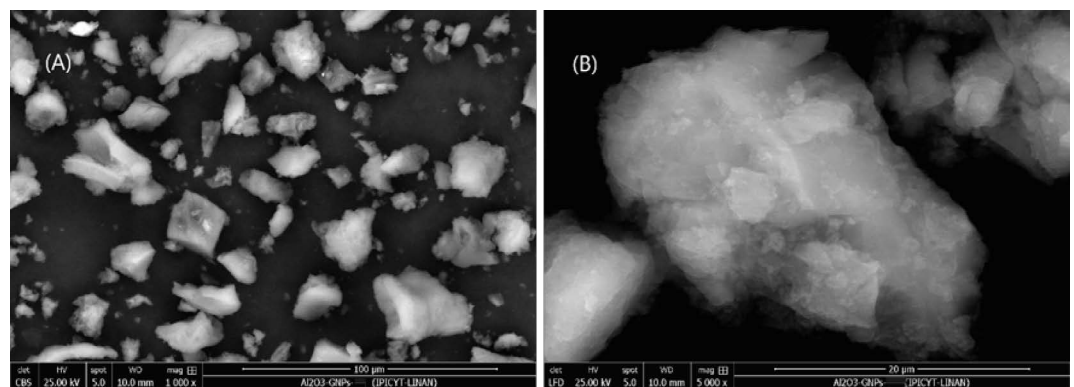**Figure 4**. SEM micrographs of TiO_2 at 2500X magnification in A and 20 000X in B.

Figure 5. SEM Micrograph of Al_2O_3/GnPs 1% at 2000X magnification in A and 5000X in B.

As in Figure 6A is shown, titanium oxide was grown on the surface of GnPs. The morphology of the accumulated TiO_2 particles is semispherical, with sizes between 501 and 286 nm (Figure 6B).
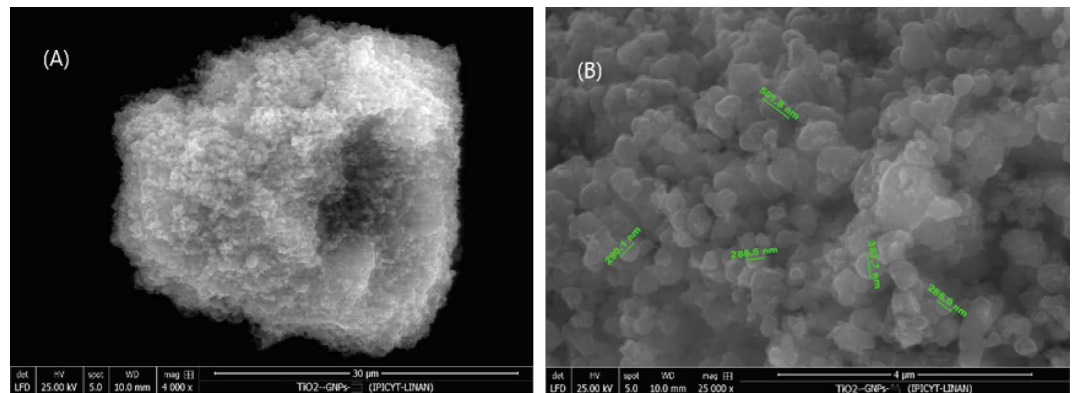
Figure 6. SEM micrograph of TiO_2/GnPs 1% at 4000X magnification in A and 25000X in B.

Figure 7A shows SEM micrograph of TiO_2-Al_2O_3/GnPs 1%, it can be observed that part of the graphene nanoplatelets was well dispersed in the TiO_2-Al_2O_3 binary mixture. However, no preferential arrangement of the nanoplatelets in the binary matrix was observed in both vertical and horizontal directions (Figure 7B).

Results of Uv-Vis analysis are shown in Figure 8. The Al_2O_3 UV-Vis spectrum corresponds to typically insulating material. The TiO_2 spectrum is like that reported in the literature, with an absorption maximum at 400 nm wavelength (Raja *et al.*, 2006). The corresponding GnPs films, in turn, showed a linear trend in absorbance.

Incorporation of GnPs into TiO_2 resulted in a higher absorption capacity than that of the pure GnPs. However, the GnPs have a different effect on alumina, *i.e.*, the absorption capacity was favored, which is a function of the GnPs concentration in sample.

On the other hand, the titanium-aluminum mixture showed a shift to lower wavelengths (370 nm), according to the absorption of the titanium oxide reference. The sample TiO_2-Al_2O_3/GnPs 1wt% presented an absorbance near 420 nm, slightly higher than TiO_2. Based on the spectra, the band gap of all materials was calculated using Tauc's method (Tauc, 1987); the results are shown in Table 2.

TiO_2 band gap resulted to be close to that reported in the literature (Kim *et al.*, 2011), and decreased when GnPs were incorporated. In the case of Al_2O_3-GnPs, calculated band gap was like that obtained for titanium oxide. There is no change in the band gap when
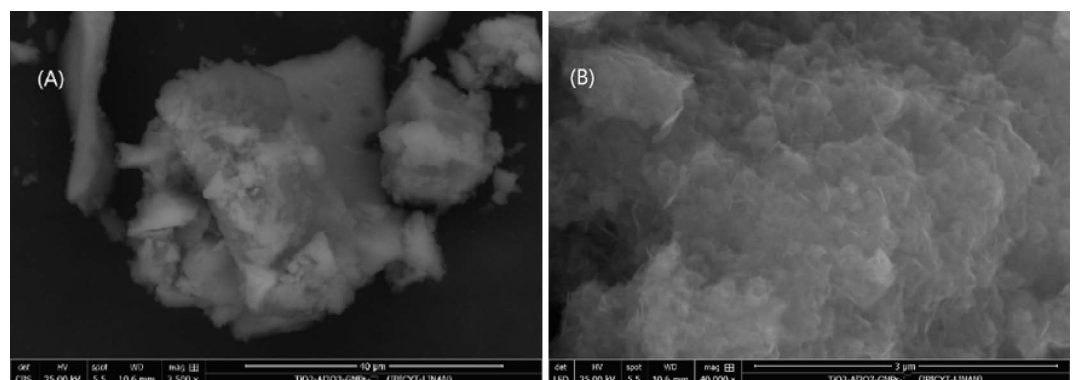

Figure 7: SEM micrograph of TiO_2-Al_2O_3/GnPs 1% at 2500X magnification in A and 40 000X in B.
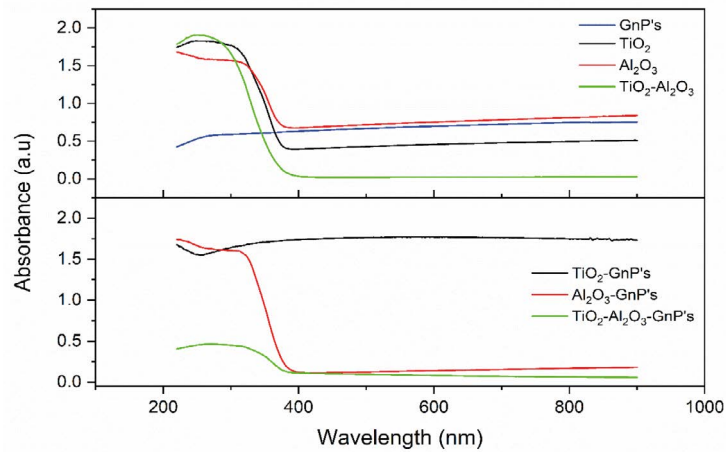
Figure 8. UV-Vis spectra for powder samples.

integrating aluminum and titanium oxide together. However, 1% GnfPs in the binary mixture reduced the gap by 6%.

A solution was prepared at 30 ppm of Diuron, from which 250 mL was taken and poured into the photoreactor, and then 0.01mg of the catalyst were added as well. The equilibrium stage consisted of keeping the catalyst in contact with the Diuron solution during 1 h. Subsequently, a 5 mL aliquot was taken as a reference (concentration at zero time). Once this stage was completed, the simulator was turned on; aliquots were taken at 5, 15, 30, 30, 45, 60, 60, 120, 180, 240, and 300 min of reaction time, UV-Vis reading followed the contaminant. A calibration curve was previously performed.

Figure 9 shows results of the normalized Diuron concentration in the photodegradation process. Upon probing the reference materials, considerable decrease in concentration due to the photolysis was observed, but alumina presented the least decrease. Binary mixtures presented slow concentration decrease w.r.t. TiO_2-Al_2O_3/GnPs 1%, also showed the smallest decrease in concentration.
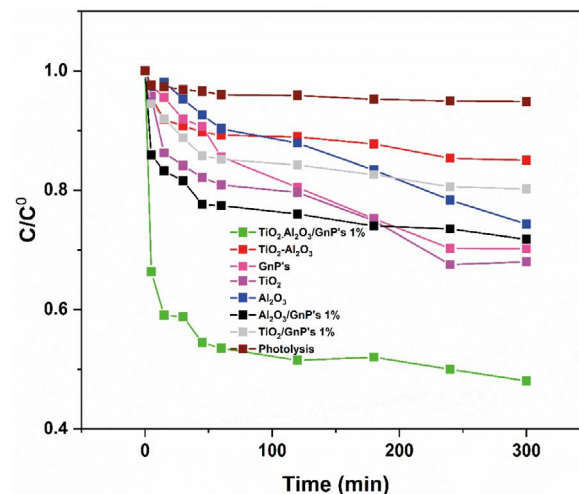

Figure 9. Normalized Diuron concentration *vs.* reaction time for reference materials, binary, and ternary samples.

TiO_2-Al_2O_3/GnPs 1% showed the highest conversion, while the lowest when TiO_2-Al_2O_3 was probed. The kinetic constant (k) was calculated to compare the photocatalytic activity of all materials as well. The results are shown in Table 2.

Finally, the TiO_2-Al_2O_3/GnPs 1% sample presented a fast and constant drop out of convention throughout the reaction. According to the values of the constant kinetic k, the activity showed the following trend: TiO_2-Al_2O_3 /GnPs 1%.>Al_2O_3/GnPs 1% >TiO_2> TiO_2/GnPs 1%>TiO_2-Al_2O_3>GnPs>Al_2O_3.

If it's assumed that due to the interaction among the three species in ternary material (TiO_2-Al_2O_3/GnPs) band gap was narrowed, and that the recombination of electron-hole pairs was apparently mitigated by Al_2O_3 presence, then the photocatalytic activity of ternary mixture was favored by a type II heterojunction.

Such heterojunction consists of interactions between two semiconductors with very similar band gaps. Consequently, photo-excited electrons are transferred from the conduction band of component A (GnPs) to the conduction band of component B (TiO_2), and the holes can travel in the opposite direction of the electrons. In addition, the insulator (Al_2O_3) helps to avoid recombination by enhancing electron trapping. This type of interface reduces the band gap and generates an efficient charge separation by decreasing the recombination rate, and then improving the photocatalytic activity in the materials. Figure 10 schematizes the heterojunction propitiated for the ternary material.

Table 2. Crystal size and band gap of materials, and herbicide conversion rates.

Sample	Crystal size (nm)	Band gap (eV)	k (h^{-1})[a]	x (%)[b]
TiO_2	3.19	3.0	0.55	32
Al_2O_3	11.08	---	0.06	26
GnPs	-	1.7	0.17	30
TiO_2-Al_2O_3	7.03	2.5	0.30	15
TiO_2/GnPs 1%	10.76	3.0	0.31	20
Al_2O_3/GnPs 1%	10.36	3.0	0.60	28
TiO_2-Al_2O_3/GnPs 1%	9.05	2.8	1.81	52

[a] Apparent kinetic constant
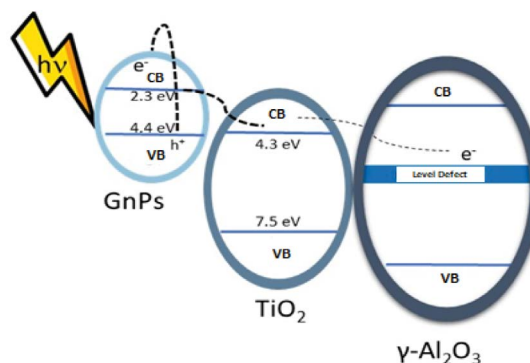[b] Conversion (x) to 300 min of reaction time

Figure 10. Scheme of photoactivity and heterojunction of ternary material.

CONCLUSIONS

The sol-gel method allowed the synthesis of the mixed oxide (titanium oxide-aluminum oxide). The presence the GnPs crystal structure was reflected in the texture of the resulting material. The interactions between the species had a positive effect on the electronic properties of the mixed oxide. The incorporation of GnPs into the mixed oxide influenced the fine structure of the product. However, the textural properties were modified by increasing the surface area and incorporating new porosity. The distribution of GnPs in the mixed oxide was random. Electronic properties such as band gap were slightly reduced. The properties modified by GnPs presence were of great relevance in the photoactivity because a heterojunction regales the electron-hole pairs and, consequently, the higher activity yield in the degradation of Diuron.

ACKNOWLEDGMENT

REFERENCES

Anderson, C., & Bard, A. J. (1997). Improved photocatalytic activity and characterization of mixed TiO_2/SiO_2 and TiO_2/Al_2O_3 materials. *Journal of Physical Chemistry B, 101*(14), 2611-2616. https://doi.org/10.1021/jp9626982

Araña, J., Peña Alonso, A., Doña Rodríguez, J. M., Herrera Melián, J. A., González Díaz, O., & Pérez Peña, J. (2008). Comparative study of MTBE photocatalytic degradation with TiO_2 and Cu-TiO_2. *Applied Catalysis B: Environmental, 78*(3-4), 355-363. https://doi.org/10.1016/j.apcatb.2007.09.023

Bamba, D., Atheba, P., Robert, D., Trokourey, A., & Dongui, B. (2008). Photocatalytic degradation of the diuron pesticide. *Environmental Chemistry Letters, 6*(3), 163-167. https://doi.org/10.1007/s10311-007-0118-x

Bernardes, A. A., Salcedo, G. M., Jorge, M. B., Bianchini, A., Wolke, S. I., & Primel, E. G. (2016). *Photocatalytic Degradation for Treating Multipesticide Residues Using [Ru(bipy) 3] Cl$_2$ -Doped TiO$_2$/SiO$_2$ Based on Surface Response Methodology. 27*(12), 2256-2263.

Campos, C. H., Torres, C., Fierro, J. L. G., & Reyes, P. (2013). Enantioselective hydrogenation of 1-phenyl-1,2-propanedione over Pt on immobilized cinchonidine on γ-Al_2O_3 catalysts. *Applied Catalysis A: General, 466*, 198-207. https://doi.org/10.1016/j.apcata.2013.06.036

Choi, H., Stathatos, E., & Dionysiou, D. D. (2006). Sol-gel preparation of mesoporous photocatalytic TiO_2 films and TiO_2/Al_2O_3 composite membranes for environmental applications. *Applied Catalysis B: Environmental, 63*(1-2), 60-67. https://doi.org/10.1016/j.apcatb.2005.09.012

Cruz, D. De, Arévalo, J. C., Torres, G., Margulis, R. G. B., Ornelas, C., & Aguilar-elguézabal, A. (2011). TiO_2 doped with Sm^{3+} by sol – gel: Synthesis, characterization and photocatalytic activity of diuron under solar light. *Catalysis Today, 166*(1), 152-158. https://doi.org/10.1016/j.cattod.2010.08.023

Cruz, M., Gomez, C., Duran-Valle, C. J., Pastrana-Martínez, L. M., Faria, J. L., Silva, A. M. T., Faraldos, M., & Bahamonde, A. (2017). Applied Surface Science Bare TiO_2 and graphene oxide TiO_2 photocatalysts on the degradation of selected pesticides and influence of the water matrix . *Applied Surface Science, 416*, 1013-1021. https://doi.org/10.1016/j.apsusc.2015.09.268

Cychosz, K. A., Guillet-Nicolas, R., García-Martínez, J., & Thommes, M. (2017). Recent advances in the textural characterization of hierarchically structured nanoporous materials. *Chemical Society Reviews, 46*(2), 389-414. https://doi.org/10.1039/C6CS00391E

Daş, E., Kaplan, B. Y., Gürsel, S. A., & Yurtcan, A. B. (2019). Graphene nanoplatelets-carbon black hybrids as an efficient catalyst support for Pt nanoparticles for polymer electrolyte membrane fuel cells. *Renewable Energy, 139*, 1099-1110. https://doi.org/10.1016/j.renene.2019.02.137

Escobar, J., De Los Reyes, J. A., & Viveros, T. (2000). Influence of the synthesis additive on the textural and structural characteristics of sol-gel Al_2O_3-TiO_2. *Industrial and Engineering Chemistry Research, 39*(3), 666-672. https://doi.org/10.1021/ie990487o

Fenoll, J., Sabater, P., Navarro, G., Pérez-Lucas, G., & Navarro, S. (2013). Photocatalytic transformation of sixteen substituted phenylurea herbicides in aqueous semiconductor suspensions: Intermediates and degradation pathways. *Journal of Hazardous Materials*, 244-245, 370-379. https://doi.org/10.1016/j.jhazmat.2012.11.055

Giacomazzi, S., & Cochet, N. (2004). Environmental impact of diuron transformation: A review. *Chemosphere, 56*(11), 1021-1032. https://doi.org/10.1016/j.chemosphere.2004.04.061

Kim, H., Kim, J., Kim, W., & Choi, W. (2011). *Enhanced Photocatalytic and Photoelectrochemical Activity in the Ternary Hybrid of CdS / TiO$_2$ / WO$_3$ through the Cascadal Electron Transfer*. 9797-9805.

Malato, S., Cáceres, J., Fernández-Alba, A. R., Piedra, L., Hernando, M. D., Agüera, A., & Vial, I. (2003). Photocatalytic treatment of diuron by solar photocatalysis: Evaluation of main intermediates and toxicity. *Environmental Science and Technology, 37*(11), 2516-2524. https://doi.org/10.1021/es0261170

Navarrete, J., Lopez, T., Gomez, R., & Figueras, F. (1996). Surface acidity of sulfated TiO$_2$-SiO$_2$ sol-gels. *Langmuir, 12*(18), 4385-4390. https://doi.org/10.1021/la950927q

Nguyen, C. H., Tran, M. L., Tran, T. T. Van, & Juang, R. S. (2020). Enhanced removal of various dyes from aqueous solutions by UV and simulated solar photocatalysis over TiO$_2$/ZnO/rGO composites. *Separation and Purification Technology, 232*(August 2019). https://doi.org/10.1016/j.seppur.2019.115962

Publishing, I. W. A., & Science, W. (2017). *Effect of W doping level on TiO$_2$ on the photocatalytic degradation of Diuron Ghania Foura, Ahcène Soualah and Didier Robert. 3*, 20-27. https://doi.org/10.2166/wst.2016.472

Raja, K. S., Misra, M., Mahajan, V. K., Gandhi, T., Pillai, P., & Mohapatra, S. K. (2006). Photo-electrochemical hydrogen generation using band-gap modified nanotubular titanium oxide in solar light. *Journal of Power Sources, 161*(2), 1450-1457. https://doi.org/10.1016/j.jpowsour.2006.06.044

Rey, A., Álvarez, P. M., Beltrán, F. J., & Puma, G. L. (2015). *Applied Catalysis B : Environmental Boron doped TiO$_2$ catalysts for photocatalytic ozonation of aqueous mixtures of common pesticides: Diuron, o-phenylphenol, MCPA and terbuthylazine. 178*, 74-81. https://doi.org/10.1016/j.apcatb.2014.10.036

Richard Felder. (2004). Principios Elementales de los Procesos Químicos (3rd ed.). Limusa Wiley.

Scherrer, P. K., & Hillberry, B. M. (1978). Determining distance to a surface represented in piecewise fashion with surface patches. *Computer-Aided Design, 10*(5), 320-324. https://doi.org/10.1016/0010-4485(78)90034-9

Tahir, M., Siraj, M., Tahir, B., Umer, M., Alias, H., & Othman, N. (2020). Au-NPs embedded Z–scheme WO$_3$/TiO$_2$ nanocomposite for plasmon-assisted photocatalytic glycerol-water reforming towards enhanced H2 evolution. *Applied Surface Science, 503*, 144344. https://doi.org/10.1016/j.apsusc.2019.144344

Tang, L., Zhao, Z., Li, K., Yu, X., Wei, Y., Liu, J., Peng, Y., Li, Y., & Chen, Y. (2020). Highly Active Monolith Catalysts of LaKCoO$_3$ Perovskite-type Complex Oxide on Alumina-washcoated Diesel Particulate Filter and the Catalytic Performances for the Combustion of Soot. *Catalysis Today, 339*, 159-173. https://doi.org/10.1016/j.cattod.2019.07.039

Tauc, J. (1987). Band tails in amorphous semiconductors. *Journal of Non-Crystalline Solids*, 97-98, 149-154. https://doi.org/10.1016/0022-3093 (87)90035-4

Thurman, E. M., Bastian, K. C., & Mollhagen, T. (2000). Occurrence of cotton herbicides and insecticides in playa lakes of the High Plains of West Texas. *Science of The Total Environment, 248*(2-3), 189-200. https://doi.org/10.1016/S0048-9697 (99)00542-2

Urbano, M. A. V., Muñoz, Y. H. O., Fernández, Y. O., Mosquera, P., Páez, J. E. R., & Amado, R. J. C. (2011). Nanopartículas de TiO$_2$, fase anatasa, sintetizadas por métodos químicos. 16

Wessels, J.S.C., & Van der Veen, R. (1956). The action of some derivatives of phenylurethan and of 3, phenyl-1,1-dimethylurea on Hill reaction. *Biochem. Biophys, 19*(3), 548-549. https://doi.org/10.1016/0006-3002 (56)90481-4